Title Page

Synthesis and evaluation of a radioiodinated peptide probe targeting αvβ6 integrin for the detection of pancreatic ductal adenocarcinoma

Masashi Ueda[a,b,1], Takahiro Fukushima[b], Kei Ogawa[b], Hiroyuki Kimura[b,c], Masahiro Ono[b], Takashi Yamaguchi[d], Yuzuru Ikehara[d], Hideo Saji[b]

[a] Radioisotopes Research Laboratory, Kyoto University Hospital, Faculty of Medicine, Kyoto University, Kyoto 606-8507, Japan

[b] Department of Patho-Functional Bioanalysis, Graduate School of Pharmaceutical Sciences, Kyoto University, Kyoto 606-8501, Japan

[c] Radioisotope Research Center of Kyoto University, Kyoto 606-8501, Japan

[d] Molecular Medicine Team, Research Center for Medical Glycoscience, National Institute of Advanced Industrial Science and Technology (AIST), Tsukuba 305-8568, Japan

[1]Current address: Department of Pharmaceutical Analytical Chemistry, Graduate School of Medicine, Dentistry, and Pharmaceutical Sciences, Okayama University, Okayama 700-8530, Japan

Corresponding author:

Hideo Saji, Ph.D.

Department of Patho-Functional Bioanalysis

Graduate School of Pharmaceutical Sciences

Kyoto University

46-29 Yoshida Shimoadachi-cho, Sakyo-ku, Kyoto 606-8501, Japan

Phone: +81-75-753-4556; Fax: +81-75-753-4568

E-mail: hsaji@pharm.kyoto-u.ac.jp

Abstract

Introduction: Pancreatic ductal adenocarcinoma (PDAC) remains a major cause of cancer-related death. Since significant upregulation of αvβ6 integrin has been reported in PDAC, this integrin is a promising target for PDAC detection. In this study, we aimed to develop a radioiodinated probe for the imaging of αvβ6 integrin-positive PDAC with single-photon emission computed tomography (SPECT).

Methods: Four peptide probes were synthesized and screened by competitive and saturation binding assays using 2 PDAC cell lines (AsPC-1, αvβ6 integrin-positive; MIA PaCa-2, αvβ6 integrin-negative). The probe showing the best affinity was used to study the biodistribution assay, an *in vivo* blocking study, and SPECT imaging using tumor bearing mice. Autoradiography and immunohistochemical analysis were also performed.

Results: Among the 4 probes examined in this study, ^{125}I-IFMDV2 showed the highest affinity for αvβ6 integrin expressed in AsPC-1 cells and no affinity for MIA PaCa-2 cells. The accumulation of ^{125}I-IFMDV2 in the AsPC-1 xenograft was 3−5 times greater than that in the MIA PaCa-2 xenograft, consistent with the expression of αvβ6 integrin in each xenograft, and confirmed by immunohistochemistry. Pretreatment with excess amounts of A20FMDV2 significantly blocked the accumulation of ^{125}I-IFMDV2 in the AsPC-1 xenograft, but not in the MIA PaCa-2 xenograft. Furthermore, ^{123}I-IFMDV2 enabled clear visualization of the AsPC-1 xenograft.

Conclusion: ^{123}I-IFMDV2 is a potential SPECT probe for the imaging of αvβ6 integrin in PDAC.

Keywords:

αvβ6 integrin; Pancreatic ductal adenocarcinoma; Small animal SPECT/CT; Nuclear medical imaging

1. Introduction

Pancreatic ductal adenocarcinoma (PDAC) remains a major cause of cancer-related death, despite advances in surgical and medical care [1]. The majority of the patients present with locally advanced or metastatic disease and die within 6–12 months. Unfortunately, most cases of PDAC are diagnosed at an advanced stage, when the disease has spread and is not amenable to surgical intervention, leading to dismal survival rates [2]. This can be explained by the fact that early PDAC is minimally symptomatic and lacks specific clinical features. Thus, development of a method for PDAC detection at an early stage is desirable.

The αvβ6 integrin is an epithelial-specific integrin and usually not detectable on non-pathologic tissues. It is significantly upregulated by many cancers and is identified as a prognostic marker [3,4]. The expression of αvβ6 integrin was strongest in PDAC among other gastrointestinal adenocarcinomas and significant upregulation of αvβ6 integrin has been linked to malignancy of PDAC [5]. These data suggest that αvβ6 integrin is a promising target for not only detection but also prognosis of PDAC.

The αvβ6 integrin binds to the arginine-glycine-aspartate (RGD) motif in its ligand, which includes fibronectin and tenascin. Furthermore, recent studies confirmed the importance of the DLXXL region in αvβ6-dependent binding, where L indicates leucine and X indicates the location of a nonspecific amino acid [6]. Several peptides containing such motif (A20FMDV2 [7], TP H2009.1 [8], Bpep [9], and Peptide 29 [10]) have been identified by phage display screening to bind specifically to αvβ6 integrin. However, the binding affinity of each peptide was not evaluated quantitatively except for A20FMDV2, which showed nM-order affinity to αvβ6 integrin and has already been labeled with ^{18}F and ^{64}Cu for positron emission tomography (PET) imaging

[7,11,12] and with ^{111}In for single-photon emission computed tomography (SPECT) imaging [13]. To our knowledge, imaging probes based on the other 3 peptides have not been developed.

Although an ^{111}In-labeled A20FMDV2 probe for SPECT imaging has already been developed, no radioiodinated peptide probes targeting αvβ6 integrin have been reported so far. In terms of half-life, the specific activity of ^{123}I is higher than that of ^{111}In. A probe with higher specific activity can produce an image with enhanced contrast. Thus, we aimed to develop a ^{123}I-labeled peptide probe to visualize αvβ6-integrin-positive PDAC by SPECT. Since the introduction of ^{18}F- or ^{64}Cu-labeling sites to the N-terminus of A20FMDV2 did not affect the binding to αvβ6 integrin, glycylcysteine was introduced at the N-terminus of each peptide to label site-specifically using *N*-(*m*-[$^{123/125}$I]iodophenyl)maleimide (IPM). The binding affinity of the IPM-conjugated peptides obtained was measured, and then the peptide showing the highest affinity was utilized for the *in vivo* evaluation as an αvβ6 integrin imaging probe.

2. Materials and Methods

2.1. Peptide synthesis

The 9-fluorenylmethyloxycarbonyl (Fmoc)-protected amino acids and Fmoc-NH-SAL-PEG Resin were purchased from Watanabe Chemical Industries, Ltd. (Hiroshima, Japan). A20FMDV2 and GC-A20FMDV2 were automatically synthesized by Fmoc solid-phase peptide synthesis and the conjugation of the peptides and IPM was performed according to a previously described method [14]. Other IPM-conjugated peptides (Table 1) were purchased from BEX Co., Ltd. (Tokyo, Japan) and KNC Laboratories Co., Ltd. (Kobe, Japan).

2.2. Radiolabeling

Na[^{125}I]I was purchased from MP Biomedicals, Inc. (Santa Ana, CA). NH_4[^{123}I]I was kindly supplied from Nihon Medi-Physics Co., Ltd. (Tokyo, Japan). Radiolabeling of the peptides was performed according to a procedure described previously [14]. The radiochemical yields of ^{123}I-IFMDV2 and ^{125}I-IFMDV2 were approximately 30% and 60%, respectively. The radiochemical purity of both probes was >99% (Supplementary Fig. 1). Both probes were obtained in no-carrier-added conditions.

2.3. Cell Culture

AsPC-1 human pancreatic carcinoma cells were obtained from the European Collection of Cell Cultures (ECACC) and maintained in Roswell Park Memorial Institute medium (RPMI; Nissui Pharmaceutical Co., Ltd., Tokyo, Japan) supplemented with 10% heat-inactivated fetal bovine serum (FBS). MIA PaCa-2 human pancreatic carcinoma cells were also obtained from ECACC and maintained in Dulbecco's modified Eagle's medium (Nissui Pharmaceutical) supplemented with 10% heat-inactivated FBS. The culture media were supplemented with penicillin (100 units/mL) and streptomycin (100 μg/mL). Cells were incubated at 37°C in a well-humidified incubator with 5% CO_2 and 95% air.

2.4. Competitive binding assay

AsPC-1 cells were grown to confluency in 24-well plates and washed with PBS. ^{125}I-IFMDV2 (50 μL, no-carrier-added conditions) was incubated with a competitor peptide (varying from 1 pM to 10 μM) in a 24-well plate together with 400 μL of RPMI. The plates were

incubated at 37°C for 90 min, after which the wells were washed twice with 1 mL of ice-cold RPMI, and then the cells were lysed with 1 mL of 0.2 M NaOH for 15 min. The radioactivity of the lysates was measured on a gamma counter (Cobra 2; Packard Instruments), and the protein concentration of the lysates was determined by BCA protein assay. The 50% inhibiting concentration (IC_{50}) values were calculated by nonlinear regression analysis using GraphPad Prism 5 (GraphPad Software, Inc., San Diego, CA). Each experiment was carried out with triplicate wells and repeated 3 times.

2.5. Saturation binding assay

AsPC-1 and MIA PaCa-2 cells were grown to confluency in 24-well plates and washed with PBS. Various concentrations of ^{125}I-IFMDV2 (0.25–100 nM; specific activity, 8.14 GBq/μmol) in RPMI were added to each well. To determine non-specific binding, non-radiolabelled A20FMDV2 (10 μM) was also added to some wells. The incubation, wash, and measurement of radioactivity and protein concentration were performed in the same way as described in the *Competitive binding assay* section. The specific binding of ^{125}I-IFMDV2 was calculated by subtracting the non-specific binding from the total cell-bound radioactivity. Using non-linear regression analysis with GraphPad Prism, the equilibrium dissociation constant (Kd) values were determined. Each experiment was carried out with triplicate wells and repeated 3 times.

2.6. Animal Model

Animal studies were conducted in accordance with our institutional guidelines, and the

experimental procedures were approved by the Kyoto University Animal Care Committee. Male severe combined immunodeficiency mice (C.B-17/Icr-scid/scid Jcl) at 5 weeks of age were purchased from CLEA Japan, Inc. and kept at a constant ambient temperature with a 12-h light/dark cycle and free access to food and water. Models of AsPC-1 and MIA PaCa-2 tumors were prepared using subcutaneous injections of AsPC-1 cells (1.5×10^6 cells in 100 μL PBS; right shoulder) and MIA PaCa-2 cells (2×10^6 cells in 100 μL PBS; left shoulder). Approximately 1 month after the implantation, the mice were subjected to a tracer study. The average diameter of the tumors was 10 mm.

2.7. Biodistribution

^{125}I-IFMDV2 (37 kBq) was injected intravenously into tumor-bearing mice (n = 4); the mice were killed at 10, 60, 120, and 240 min after ^{125}I-IFMDV2 administration. Whole organs were immediately harvested and weighed, and their radioactivity was measured. The results were expressed as the percentage injected dose per gram (%ID/g) except for the neck (%ID).

To confirm that the probe was taken up specifically by αvβ6 integrin, ^{125}I-IFMDV2 (0.017 nmol/37 kBq; no-carrier-added conditions) was injected with or without an excess amount of non-radiolabelled A20FMDV2 (20 nmol) into tumor-bearing mice (n = 6−7). Biodistribution was determined 1 h post-injection according to the same method described above.

2.8. SPECT/X-ray computed tomography (CT) imaging

An FX3300 pre-clinical imaging system equipped with a FLEX Triumph multi-modality pre-clinical imaging platform (Gamma Medica, Inc., Northridge, CA) was used to acquire and

process the SPECT and CT data. Mice bearing AsPC-1 xenografts were given intravenous injections ranging from 28 to 45 MBq of ^{123}I-IFMDV2 in a volume of 120 μL (n = 3). At 40 min after administration, the mice were anesthetized with 1.5% isoflurane, and tomographic spiral SPECT scans were performed for 40 min using a 4-head detector camera. Immediately after SPECT acquisition, CT acquisition of the anesthetized mice was performed. The acquisition and reconstruction of images were performed according to a previously described method [15]. After CT acquisition, the mice were euthanized by exsanguination. Blood was collected and tumors were harvested and weighed immediately, and their radioactivity was measured.

2.9. Autoradiography and histological analysis

The tumors were removed and frozen in hexane (−80°C) at 1 h after a ^{123}I-IFMDV2 (10.5 MBq) injection. The frozen tumor samples were sliced into 20-μm–thick sections and adjacent 4-μm–thick sections with a cryomicrotome (CM1900 Cryostat; Leica Microsystems, Wetzlar, Germany). Autoradiograms were obtained and analyzed according to the previously described method [16].

The serial 4-μm–thick sections were subjected to hematoxylin–eosin (HE) staining and detection with an anti-αvβ6 mouse mAb (Millipore). For specific detection of the immune reactions, we employed a MOM kit (Vector Laboratories Inc., Burlingame, CA), and then incubated with 10 μg/mL anti-αvβ6 mAb at 4°C for 10 h followed by a secondary antibody, Alexa Fluor 488-labelled anti-mouse IgG (Life Technologies, Carlsbad, CA) for 1 h at room temperature. Hoechst33342 (Life Technologies) was used for nuclear staining. The slides were mounted in Prolong Gold antifade reagent (Life Technologies), and photo data were acquired using a TCS

SP5II confocal microscope (Leica Microsystems).

2.10. Statistical analyses

The data are expressed as mean ± SD. A Mann–Whitney *U* test was performed to evaluate statistical significance. A *P* value of less than 0.05 was considered statistically significant.

3. Results

3.1. Competitive binding assay

The affinity-related IC_{50} values are shown in Table 2. A20FMDV2 showed the highest affinity for AsPC-1 cells. The affinity of IFMDV2 was slightly lower than that of A20FMDV2 but still on the order of 10 nM. On the other hand, other probes had more than 10 times less affinity than A20FMDV2. The αvβ3 integrin-targeting peptide (cyclo-RGDfK; ABX GmbH, Radeberg, Germany) did not inhibit the binding of ^{125}I-IFMDV2 to AsPC-1 cells.

3.2. Saturation binding assay

The specific binding data and saturation curves are shown in Fig. 1A. The binding of ^{125}I-IFMDV2 to AcPC-1 cells was increased in a dose-dependent manner and the Kd value was determined to be 6.6 ± 2.0 nM. In contrast, ^{125}I-IFMDV2 showed no affinity for MIA PaCa-2 cells. Western blot analysis confirmed remarkable αvβ6 integrin expression in AsPC-1 cells while no obvious αvβ6 integrin expression was observed in MIA PaCa-2 cells (Fig. 1B).

3.3. Biodistribution studies

A high level of radioactivity accumulated in the kidneys and liver 10 min after injection, but it reduced rapidly. In contrast, the level of radioactivity in the intestine increased sequentially, which suggests that part of the administered ^{125}I-IFMDV2 is excreted in bile. The uptake of ^{125}I-IFMDV2 in the AsPC-1 xenograft was more than 3 times higher than that in the MIA PaCa-2 xenograft, and the AsPC-1-to-blood and AsPC-1-to-muscle ratios were greater than 1 for all time points examined (Table 3). Pretreatment with excess A20FMDV2 induced a 62% decrease in ^{125}I-IFMDV2 accumulation in the AsPC-1 xenograft. On the other hand, the radioactivity in blood and MIA PaCa-2 xenograft was not affected significantly (Fig. 2).

3.4. SPECT/CT imaging

The AsPC-1 xenograft was clearly visualized 1 h after the ^{123}I-IFMDV2 injection (Fig. 3). The radioactivity accumulated in the AsPC-1 xenografts at the end of the SPECT acquisition, i.e., 80 min after injection of ^{123}I-IFMDV2, was 0.74 ± 0.43 %ID/g. The tumor-to-blood ratio was 1.73 ± 0.56.

3.5. Autoradiography and histological analysis

Autoradiographic images of ^{123}I-IFMDV2 are shown in Fig. 4 (A: AsPC-1, B: MIA PaCa-2) and both images are at the same scale. HE staining revealed that there was 1 large tumor cell nest in Fig. 4C (AsPC-1) and there were large and small tumor cell nests in Fig. 4D (MIA PaCa-2). ^{123}I-IFMDV2 strongly accumulated in the AsPC-1 xenograft, but rarely accumulated in

the MIA PaCa-2 xenograft. The arrowhead indicates a necrotic area in the MIA PaCa-2 sample, and radioactivity was retained in the area. On immunohistochemistry, αvβ6 integrin was markedly expressed in AsPC-1, while hardly detected in MIA PaCa-2 (Fig. 4E and F).

4. Discussion

The purpose of the present study was to develop a radioiodinated peptide probe targeting αvβ6 integrin. After *in vitro* screening, we found that ^{125}I-IFMDV2 had a high affinity and selectivity for αvβ6 integrin. The *in vivo* accumulation of ^{125}I-IFMDV2 in αvβ6 integrin-positive tumors was greater than that in αvβ6 integrin-negative tumors. The accumulation was significantly blocked by pretreatment with an excess amount of A20FMDV2, indicating the specific binding of ^{125}I-IFMDV2 to αvβ6 integrin *in vivo*. Furthermore, ^{123}I-IFMDV2 could clearly visualize the αvβ6 integrin-positive tumor. These findings suggest that ^{123}I-IFMDV2 is a potential probe for SPECT imaging of αvβ6 integrin-positive tumors.

Although ^{123}I-IFMDV2 is the first radioiodinated probe targeting αvβ6 integrin, several probes containing the same amino acid sequence, i.e., A20FMDV2, and labeled with other radionuclides have already been developed. The accumulation of ^{123}I-IFMDV2 (1.31%ID/g at 1 h) in tumors was superior to that of ^{18}F-A20FMDV2 (0.66%ID/g at 1 h) [7], but inferior to that of ^{111}In-DTPA-A20FMDV2 (2.1%ID/g at 1 h) [13]. One reason for this may be the difference in binding affinity to αvβ6 integrin. Although the Kd value of ^{123}I-IFMDV2 (6.6 nM) was sufficiently high for successful SPECT imaging, it was 4-fold lower than that of ^{111}In-DTPA-A20FMDV2 (1.7 nM) [13]. Another reason may be the difference in intracellular

retention of the probes. Duncan and Welch reported that ^{111}In-DTPA-polypeptides were delivered to the lysosome after internalization, following which they were retained within the lysosome and were only slowly released from the cell [17]. In fact, a comparison of the biodistribution between ^{111}In-DTPA-antibody and ^{125}I-antibody revealed that the retention of ^{111}In in the tumor was significantly higher than that of ^{125}I [18].

The drawback of the ^{18}F-A20FMDV2 probe was low uptake and poor retention in the tumor (0.66%ID/g at 1 h and 0.06%ID/g at 4 h) [7]. However, the authors succeeded in improving the biodistribution of the probe by conjugating polyethylene glycol (PEG) with A20FMDV2. Radioactive probe accumulation in αvβ6 integrin-positive tumor was approximately 1.5−2.0%ID/g 1 h after injection of ^{18}F-PEG_{28}-A20FMDV2 and ^{18}F-$(PEG_{28})_2$-A20FMDV2, and continued until 4 h after the injection [19]. The accumulation of the probes in tumors was greater than that of ^{123}I-IFMDV2. Although the detailed mechanism of increased accumulation and retention in tumors has not yet been elucidated, it could be attributed to increased probe stability in plasma [20]. ^{123}I-IFMDV2 was also rapidly cleared from the tumor (1.31%ID/g at 1 h and 0.24%ID/g at 4 h) and was instable in plasma. Thus, PEGylation would be effective to increase accumulation and retention of ^{123}I-IFMDV2 in the tumor.

Integrins are transmembrane receptors that connect the extracellular matrix to the cytoskeleton, and influence the regulation of cell survival, proliferation, gene transcription, and migration. To date, 18 different α and 8 different β subunits have been identified, forming 24 different integrin receptors. Among them, αvβ3 integrin has been most extensively studied, and many probes targeting αvβ3 integrin have been developed [21,22,23]. Yoshimoto *et al*. reported the usefulness of SPECT imaging with ^{111}In-labeled c(RGDfK), an imaging probe of αvβ3

integrin, for the early detection of pancreatic cancer in a hamster model of pancreatic carcinogenesis [24]. Therefore, not only αvβ6 integrin but also αvβ3 integrin are potential targets for the detection of PDAC. However, the immunohistochemical analyses using human PDAC samples revealed that αvβ3 integrin was expressed in 29 of 50 samples [25], whereas αvβ6 integrin was expressed in 33 of 34 samples [5]. Thus, probes targeting αvβ6 integrin may detect PDAC with greater sensitivity than those targeting αvβ3 integrin. Furthermore, microarray analysis revealed that not the β3- but the β6-integrin gene was upregulated in PDAC samples with a poor outcome. Interestingly, the upregulation of the β6-integrin gene was not observed in those with a good outcome [26]. These findings suggest that probes targeting αvβ6 integrin can give information about the prognosis of PDAC.

Phage display analysis identified the DLXXL sequence as a key moiety responsible for αvβ6 specificity while having only minimal interactions with αvβ3, αvβ5, and αIIbβ3 [27]. In fact, the binding of ^{125}I-IFMDV2 to αvβ6 integrin expressed in AsPC-1 cells was not inhibited by a RGD peptide lacking a DLXXL sequence (cyclo-[RGDfK]). This finding indicates high selectivity of ^{125}I-IFMDV2 to αvβ6 integrin. Among the peptides containing the DLXXL sequence, IFMDV2 showed the highest affinity for AsPC-1 cells. We preliminarily evaluated the affinity of IPM-conjugated TP-H2009.1 and Bpep at the C-terminus, but found the affinity of those probes was lower than that of IFMDV2 (data not shown). However, these findings do not necessarily deny the possibility of using the sequences examined in this study (except for A20FMDV2) as a basic scaffold for an αvβ6 integrin targeting probe. In the present study, we screened the probes with a single prosthetic group (IPM) and a fixed length of spacer (glycine). Other prosthetic groups for radioiodination, such as *N*-succinimidyl-3-iodobenzoate [28], have

been reported. The use of different prosthetic groups and/or different kinds and lengths of spacers might lead to a useful αvβ6 integrin targeting probe containing a TP-H2009.1, Bpep, or Peptide29 sequence.

5. Conclusion

$^{123/125}$I-IFMDV2 showed high affinity and specificity for αvβ6 integrin both *in vitro* and *in vivo*. The αvβ6-integrin-positive pancreatic cancer was clearly visualized and thus, ^{123}I-IFMDV2 is a potential SPECT probe for the imaging of αvβ6 integrin in PDAC. It could bring valuable information not only for the detection of αvβ6-integrin-positive tumors but also for the evaluation of the efficacy of αvβ6-integrin targeted therapy.

Acknowledgments

The authors would like to thank Nihon Medi-Physics Co. Ltd. for providing ammonium [^{123}I]iodide. This work was supported in part by the "Research and Development Project on Molecular Probes for Detection of Biological Features on Cancer" by the New Energy and Industrial Technology Development Organization (NEDO), Japan; a Grant-in-Aid for Scientific Research (KAKENHI) from the Japan Society for the Promotion of Science; and a grant from the Pancreas Research Foundation of Japan. The authors declare no conflicts of interest.

References

[1] Siegel R, Naishadham D, Jemal A, Cancer statistics, 2012, CA Cancer J. Clin. 62 (2012) 10-29.

[2] Stan SD, Singh SV, Brand RE, Chemoprevention strategies for pancreatic cancer, Nat. Rev. Gastroenterol. Hepatol. 7 (2010) 347-356.

[3] Hazelbag S, Kenter GG, Gorter A, et al., Overexpression of the alpha v beta 6 integrin in cervical squamous cell carcinoma is a prognostic factor for decreased survival, J. Pathol. 212 (2007) 316-324.

[4] Zhang ZY, Xu KS, Wang JS, et al., Integrin alphanvbeta6 acts as a prognostic indicator in gastric carcinoma, Clin. Oncol. 20 (2008) 61-66.

[5] Sipos B, Hahn D, Carceller A, et al., Immunohistochemical screening for beta6-integrin subunit expression in adenocarcinomas using a novel monoclonal antibody reveals strong up-regulation in pancreatic ductal adenocarcinomas in vivo and in vitro, Histopathology. 45 (2004) 226-236.

[6] Burman A, Clark S, Abrescia NG, et al., Specificity of the VP1 GH loop of Foot-and-Mouth Disease virus for alphav integrins, J. Virol. 80 (2006) 9798-9810.

[7] Hausner SH, DiCara D, Marik J, et al., Use of a peptide derived from foot-and-mouth disease virus for the noninvasive imaging of human cancer: generation and evaluation of 4-[^{18}F]fluorobenzoyl A20FMDV2 for in vivo imaging of integrin alphavbeta6 expression with positron emission tomography, Cancer Res. 67 (2007) 7833-7840.

[8] Elayadi AN, Samli KN, Prudkin L, et al., A peptide selected by biopanning identifies the integrin alphavbeta6 as a prognostic biomarker for nonsmall cell lung cancer, Cancer Res.

67 (2007) 5889-5895.

[9] Pameijer CR, Navanjo A, Meechoovet B, et al., Conversion of a tumor-binding peptide identified by phage display to a functional chimeric T cell antigen receptor, Cancer Gene Ther. 14 (2007) 91-97.

[10] Hsiao JR, Chang Y, Chen YL, et al., Cyclic alphavbeta6-targeting peptide selected from biopanning with clinical potential for head and neck squamous cell carcinoma, Head Neck. 32 (2010) 160-172.

[11] Hausner SH, Kukis DL, Gagnon MK, et al., Evaluation of [^{64}Cu]Cu-DOTA and [^{64}Cu]Cu-CB-TE2A chelates for targeted positron emission tomography with an alphavbeta6-specific peptide, Mol. Imaging. 8 (2009) 111-121.

[12] Hausner SH, Carpenter RD, Bauer N, et al., Evaluation of an integrin alphavbeta6-specific peptide labeled with [^{18}F]fluorine by copper-free, strain-promoted click chemistry, Nucl. Med. Biol. 40 (2013) 233-239.

[13] Saha A, Ellison D, Thomas GJ, et al., High-resolution in vivo imaging of breast cancer by targeting the pro-invasive integrin alphavbeta6, J. Pathol. 222 (2010) 52-63.

[14] Ueda M, Ogawa K, Miyano A, et al., Development of an oxygen-sensitive degradable peptide probe for the imaging of hypoxia-inducible factor-1-active regions in tumors, Mol. Imaging Biol. 15 (2013) 713-721.

[15] Harada N, Kimura H, Ono M, et al., Preparation of Asymmetric Urea Derivatives that Target Prostate-Specific Membrane Antigen for SPECT Imaging, J Med Chem. 56 (2013) 7890-7901.

[16] Kondo N, Temma T, Shimizu Y, et al., Miniaturized antibodies for imaging membrane type-1

matrix metalloproteinase in cancers, Cancer Sci. 104 (2013) 495-501.

[17] Duncan JR, Welch MJ, Intracellular metabolism of indium-111-DTPA-labeled receptor targeted proteins, J. Nucl. Med. 34 (1993) 1728-1738.

[18] Steffens MG, Kranenborg MH, Boerman OC, et al., Tumor retention of ^{186}Re-MAG3, ^{111}In-DTPA and ^{125}I labeled monoclonal antibody G250 in nude mice with renal cell carcinoma xenografts, Cancer Biother. Radiopharm. 13 (1998) 133-139.

[19] Hausner SH, Abbey CK, Bold RJ, et al., Targeted in vivo imaging of integrin alphavbeta6 with an improved radiotracer and its relevance in a pancreatic tumor model, Cancer Res. 69 (2009) 5843-5850.

[20] Dapp S, Muller C, Garayoa EG, et al., PEGylation, increasing specific activity and multiple dosing as strategies to improve the risk-benefit profile of targeted radionuclide therapy with ^{177}Lu-DOTA-bombesin analogues, EJNMMI Res. 2 (2012) 24.

[21] Gaertner FC, Kessler H, Wester HJ, et al., Radiolabelled RGD peptides for imaging and therapy, Eur. J. Nucl. Med. Mol. Imaging. 39 Suppl 1 (2012) S126-138.

[22] Briat A, Wenk CH, Ahmadi M, et al., Reduction of renal uptake of ^{111}In-DOTA-labeled and A700-labeled RAFT-RGD during integrin alphavbeta3 targeting using single photon emission computed tomography and optical imaging, Cancer Sci. 103 (2012) 1105-1110.

[23] Zheleznyak A, Wadas TJ, Sherman CD, et al., Integrin alpha(v)beta(3) as a PET imaging biomarker for osteoclast number in mouse models of negative and positive osteoclast regulation, Mol. Imaging Biol. 14 (2012) 500-508.

[24] Yoshimoto M, Hayakawa T, Mutoh M, et al., In vivo SPECT imaging with ^{111}In-DOTA-c(RGDfK) to detect early pancreatic cancer in a hamster pancreatic

carcinogenesis model, J. Nucl. Med. 53 (2012) 765-771.

[25] Hosotani R, Kawaguchi M, Masui T, et al., Expression of integrin alphaVbeta3 in pancreatic carcinoma: relation to MMP-2 activation and lymph node metastasis, Pancreas. 25 (2002) e30-35.

[26] Van den Broeck A, Vankelecom H, Van Eijsden R, et al., Molecular markers associated with outcome and metastasis in human pancreatic cancer, J. Exp. Clin. Cancer Res. 31 (2012) 68.

[27] Kraft S, Diefenbach B, Mehta R, et al., Definition of an unexpected ligand recognition motif for alphav beta6 integrin, J. Biol. Chem. 274 (1999) 1979-1985.

[28] Nishigori K, Temma T, Yoda K, et al., Radioiodinated peptide probe for selective detection of oxidized low density lipoprotein in atherosclerotic plaques, Nucl. Med. Biol. 40 (2013) 97-103.

Table 1. Probes evaluated in this study

Name	Amino acid sequence
IPM-A20FMDV2 (IFMDV2)	C(IPM)GNAVPNLRGDLQVLAQKVART
IPM-TP H2009.1	C(IPM)GRGDLATLRQLAQEDGVVGVR
IPM-Peptide29	Cyclo-(CRGDLASLC)GGGGGGC(IPM)
IPM-Bpep	C(IPM)GRTDLDSLRTYTL

Underlines designate RG(T)DLXXL sequences.

IPM, *N*-(*m*-iodophenyl)maleimide.

Table 2. IC_{50} values of the probes

Name	IC_{50} (nM)
A20FMDV2	17 ± 2
IFMDV2	40 ± 25
IPM-TP H2009.1	420 ± 220
IPM-Peptide29	205 ± 134
IPM-Bpep	>10000
Cyclo-(RDGfK)	>10000

Values are represented as the mean ± S.D., $n = 3$.

Table 3. Biodistribution of ^{125}I-IFMDV2

Organ	Time after injection (min)			
	10	60	120	240
Blood	1.34 ± 0.10	0.44 ± 0.06	0.16 ± 0.03	0.10 ± 0.04
AsPC-1 xenograft	2.60 ± 0.68	1.31 ± 0.10	0.43 ± 0.13	0.24 ± 0.11
MIA PaCa-2 xenograft	0.83 ± 0.09	0.25 ± 0.04	0.13 ± 0.13	0.06 ± 0.06
Pancreas	2.48 ± 0.11	0.40 ± 0.10	0.19 ± 0.21	0.08 ± 0.10
Liver	7.80 ± 0.65	7.55 ± 0.63	1.57 ± 0.53	0.57 ± 0.30
Intestine	7.86 ± 1.59	11.99 ± 2.39	15.51 ± 1.82	11.61 ± 2.94
Kidneys	69.61 ± 3.31	11.10 ± 1.06	2.17 ± 0.47	1.59 ± 0.76
Muscle	1.58 ± 0.38	0.85 ± 0.08	0.38 ± 0.16	0.14 ± 0.12
Neck	0.08 ± 0.03	0.05 ± 0.02	0.04 ± 0.01	0.07 ± 0.04
AsPC-1/Blood ratio	1.96 ± 0.60	2.99 ± 0.54	2.86 ± 1.21	2.48 ± 0.75
AsPC-1/Muscle ratio	1.75 ± 0.55	1.55 ± 0.19	1.35 ± 0.67	2.03 ± 0.53

Organ uptake values are expressed as %ID/g of tissue, except in the case of the neck (%ID), and AsPC-1/Blood and AsPC-1/Muscle ratios.

Values are represented as the mean ± S.D., $n = 4$.

Figure 1

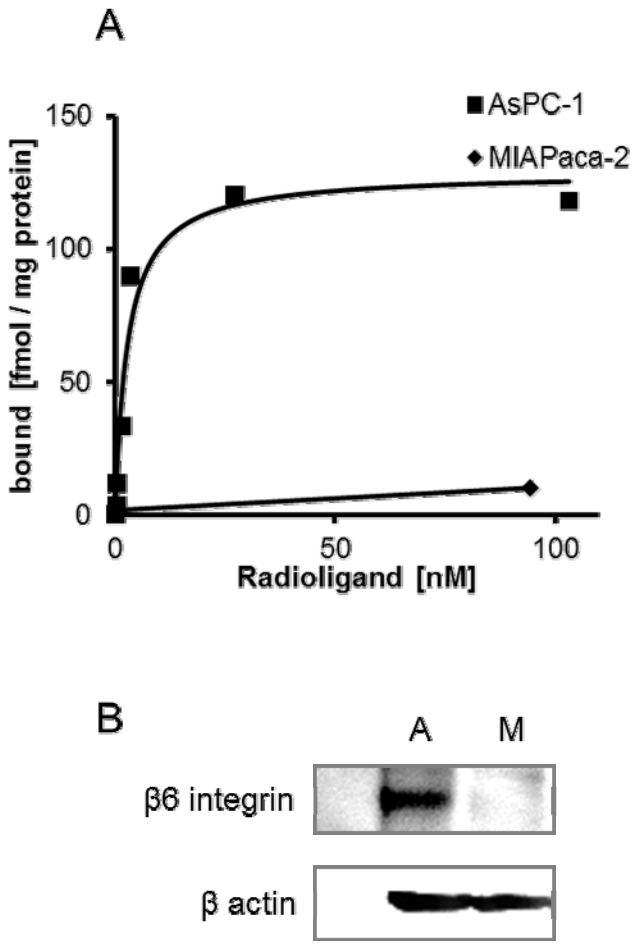

(A) Saturation binding curves of ^{125}I-IFMDV2 in AsPC-1 and MIA PaCa-2 cells. Specific binding data calculated by subtracting the non-specific binding from the total binding are shown.

(B) Western blot analysis of β6 integrin expression in AsPC-1 (Lane A) and MIA PaCa-2 (Lane M) cells. The bands of β-actin are also shown as a protein loading control.

Figure 2

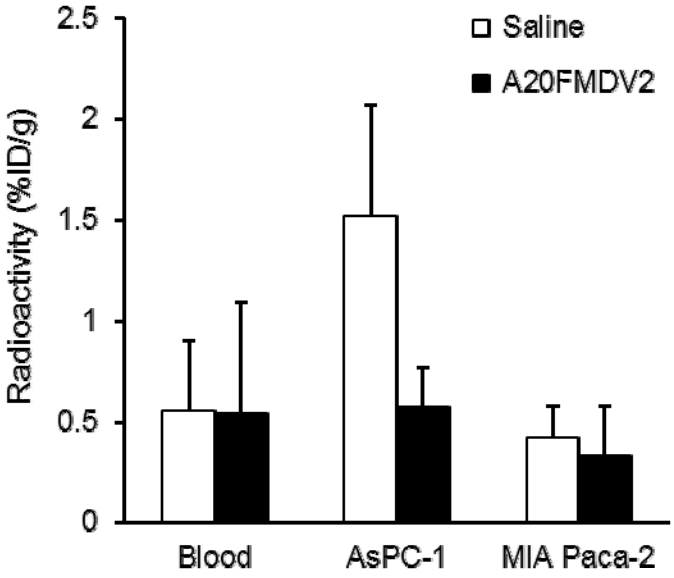

Effects of A20FMDV2 pretreatment on ^{125}I-IFMDV2 accumulation in blood, AsPC-1, and MIA PaCa-2 xenografts. Each column represents an average of 6–7 animals and each error bar represents the standard deviation. $^{**}P < 0.01$ (Mann–Whitney *U* test).

Figure 3

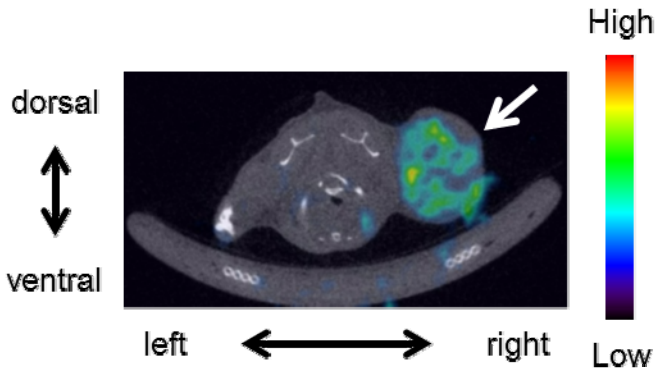

A representative SPECT/CT image of an AsPC-1-implanted mouse 1 h after injection with ^{123}I-IFMDV2. The arrow indicates the AsPC-1 xenograft.

Figure 4

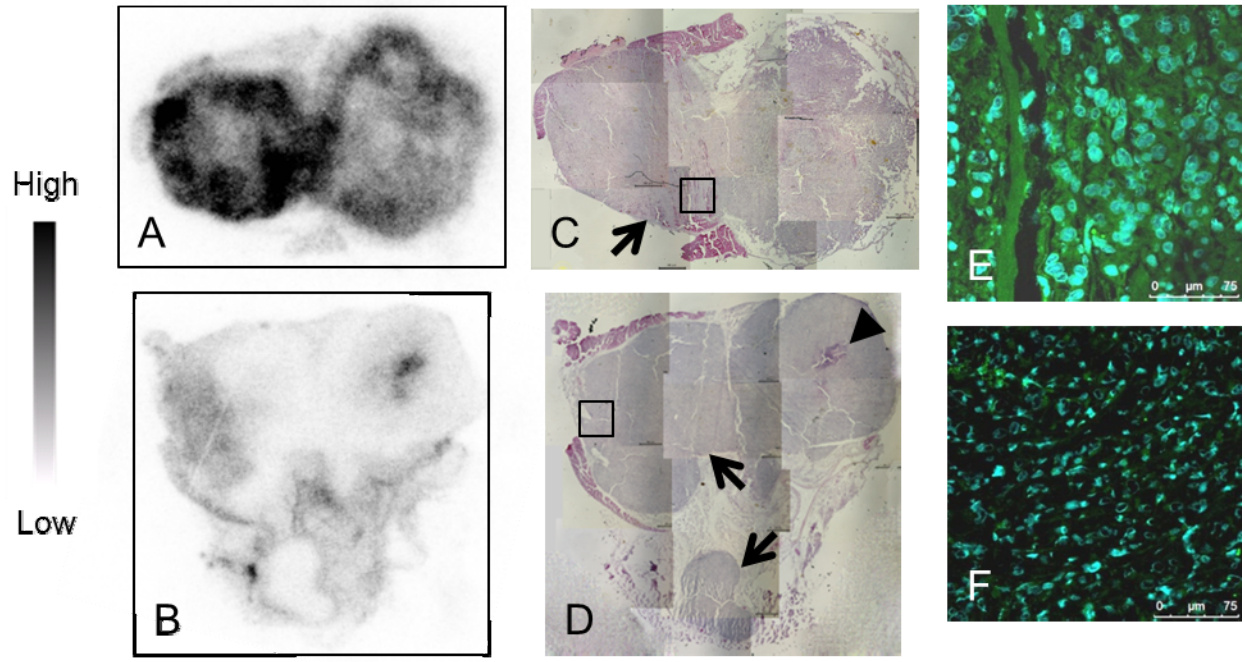

Representative images of ^{123}I-IFMDV2 autoradiograms (A, B), hematoxylin–eosin staining (C, D), and αvβ6 integrin immunostaining (E, F). Tumor sections in A, C, and E were obtained from an AsPC-1 xenograft, and those in B, D, and F were obtained from a MIA PaCa-2 xenograft. The arrows indicate tumor cell nests and the arrowhead indicates a necrotic area. The squares indicate the areas that correspond to panels E and F. αvβ6 integrin was immunostained in green and nuclei were stained in blue.

Supplementary data

Materials and Methods

Characterization of the peptides

The peptides were characterized by analytical high-performance liquid chromatography (HPLC) (5C18-AR-II column; 4.6 × 150 mm; Nacalai Tesque, Inc., Kyoto, Japan) and matrix-assisted laser desorption/ionization mass spectrometry (AXIMA-CFR Plus; Shimadzu Corporation, Kyoto, Japan) before use. The mobile phase was a linear gradient with solvent A (0.1% TFA in water) and solvent B (0.1% TFA in acetonitrile) starting at 20% solvent B and increasing to 50% over 30 min. The flow rate was 1 mL/min and the wavelength of ultraviolet detection was 220 nm.

Serum stability determination

The stability of ^{125}I-IFMDV2 was tested in mouse serum (0.3 mL). After incubation for 10, 60, and 120 min at 37°C, 50 μL of the sample was removed and mixed with 100 μL of acetonitrile. The mixture was centrifuged, and the supernatant was analyzed by HPLC under conditions described the above section. The eluent was collected every 1 min and the radioactivity was measured.

Western blotting

Whole protein was extracted from AsPC-1 and MIA PaCa-2 cells using Passive Lysis Buffer (Promega Corporation, Madison, WI) with 1% protease inhibitor. After the protein concentration of the lysates was measured using a BCA protein assay kit (Thermo Scientific,

Rockford, IL), 20 μg of protein was separated by sodium dodecylsulfate-polyacrylamide gel electrophoresis (e-PAGEL E-T/R/D520L; ATTO Corporation, Tokyo, Japan) under non-reducing conditions. Proteins were transferred to a nitrocellulose membrane (Millipore Corporation, Billerica, MA). After blocking with Blocking One (Nacalai Tesque, Inc.) at 4°C, membranes were probed with anti-β6 mouse monoclonal antibody (mAb) (Millipore). Membranes were washed 3 times for 10 min with phosphate-buffered saline (PBS) and 0.1% Tween-20 and incubated with a secondary antibody (horseradish peroxidase-conjugated goat anti-mouse IgG_3 antibody [Santa Cruz Biotechnology, Inc., Santa Cruz, CA]) for 45 min at room temperature, and the washing step was repeated. Protein bands were visualized using an ECL Plus kit (GE Healthcare UK Ltd., Buckinghamshire, UK) with a gel imaging system (ChemiDoc XRS; BIO-RAD Laboratories, Hercules, CA). Immunoblotting for β-actin was used as a protein loading control.

Results

Characterization of the peptides

A20FMDV2: calculated for $C_{93}H_{164}N_{32}O_{27}$ ($M+H^+$); m/z, 2162.52; found, 2162.80.

GC-A20FMDV2: calculated for $C_{98}H_{172}N_{34}O_{29}S$ ($M+H^+$); m/z, 2322.28; found, 2322.30.

IFMDV2: calculated for $C_{108}H_{178}IN_{35}O_{31}S$ ($M+H^+$); m/z, 2621.22; found, 2621.51.

IPM-TP H2009.1: calculated for $C_{105}H_{171}IN_{34}O_{34}S$ ($M+H^+$); m/z, 2612.74; found, 2613.49.

IPM-Peptide29: calculated for $C_{61}H_{91}IN_{20}O_{22}S_3$ ($M+H^+$); m/z, 1679.60; found, 1680.29.

IPM-Bpep: calculated for $C_{77}H_{118}IN_{21}O_{26}S$ ($M+H^+$); m/z, 1912.88; found, 1912.28.

Serum stability

The temporal changes in intact ^{125}I-IFMDV2 in mouse serum are shown in Supplementary Table 1. The radiochemical purity of ^{125}I-IFMDV2 was greater than 95% after a 10-min incubation in serum and decreased gradually in a time-dependent manner. These data are in agreement with the data reported for other probes containing the A20FMDV2 sequence.

Supplementary Table 1. Serum stability of ^{125}I-IFMDV2 *in vitro*

Incubation time (min)	Intact form (%)
10	95 ± 2
60	67 ± 25
120	50 ± 25

Values are represented as the mean ± S.D. of 3 independent examinations.

Supplementary Figure 1

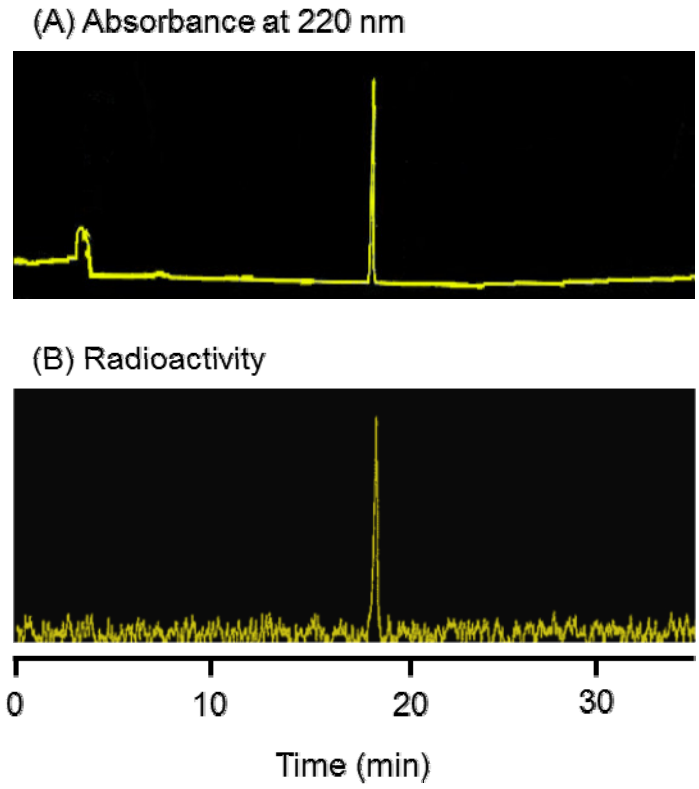

High-performance liquid chromatography profiles of nonradioactive IFMDV2 (A) and ^{125}I-IFMDV2 (B). ^{125}I-IFMDV2 showed a single peak at the retention time of 17.62 min that corresponded to the retention time of nonradioactive IFMDV2 (17.58 min).